THE JOURNAL OF PROSTHETIC DENTISTRY

RESEARCH AND EDUCATION

Physical characterization of 3 implant systems made of distinct materials with distinct surfaces

João Pimenta, DDS, DMD,[a] Serge Szmukler-Moncler, DDS, PhD,[b] and Ariel Raigrodski, DMD, MS[c]

ABSTRACT

Statement of problem. Dental implants undergo various surface treatments. Studies that have characterized their surface and subsurface by using the same methods are scarce.

Purpose. The purpose of this study is to physically characterize the surface and subsurface of implant systems made of commercially pure (cp) titanium (Ti) grade (gr) 4 and Ti alloy gr 23 and to evaluate whether airborne-particle abrasion and acid etching is an appropriate surface treatment for Ti alloy gr 23.

Material and methods. Implant groups (n=3) were as follows: TG4AO, cp Ti gr 4, treated with anodic oxidation (3.5×8 mm) (NobelReplace Conical; Nobel Biocare); TG23AE, Ti gr 23 (TiAlV ELI) airborne-particle abraded-and-etched (3.9×8 mm) (V3; MIS); and TG4AE, cp Ti gr 4, airborne-particle abraded and etched (3.3×8 mm) (BL; Institut Straumann AG). Surface roughness, surface topography, and elemental and surface composition were investigated with optical profilometry, scanning electron microscopy, energy dispersive X-ray spectroscopy, and X-ray diffraction. The presence and size of Ti hydride (TiH) needles were determined on metallographic sections. Depth profiling was obtained by time-of-flight secondary ion mass spectrometry (ToF-SIMS) to determine possible enrichment of an alloying element at the implant surface.

Results. The mean arithmetic deviation roughness (S_a), of TG4AO was 0.80 μm. The S_a of TG4AO was 1.22 μm, and the S_a of TG4AO was 1.59 μm. The difference between the groups was significant ($P<.001$). TG23AE and TG4AE displayed a macrotexture and microtexture with pores; TG4AO showed a 3-to 12-μm canyon-like structure. The surface and subsurface compositions were as follows: for TG4AO, αTi and phosphorus-rich anatase; for TG23AE, α-Ti matrix with β-Ti grains; and for TG4AE, α-Ti and δ-TiH_{2-x}. TiH needles were found only on TG4AE; the Ti oxide layer of TG4AO was rough, 3-to 16-μm thick, and porous. The time-of-flight secondary ion mass spectrometry (ToF SIMS) concentration profile of TG23AE did not show enrichment of any alloying element.

Conclusions. The roughness, topography, and composition of the surfaces were different for all implants tested. Airborne-particle abrasion and subsequent etching was an appropriate treatment for Ti gr 23 alloy implants. (J Prosthet Dent 2020;■:■-■)

Over the last 40 years, dental implants with distinct designs have been produced from different metallic materials with a large variety of surface treatments.[1-7] The aim was to increase either the level of osseointegration[5,8-10] or the biomechanical properties.[11-14]

Screw-shaped implants have been made from commercially pure (cp) titanium (Ti) from cp Ti grade (gr) 1 for the first Brånemark implants to cp Ti gr 4 of higher mechanical strength for later products.[12] To increase the fatigue mechanical properties of implants, Ti alloys have also been introduced.[6,12-14] Most of them are Ti gr 5 and Ti gr 23 made of 90% of titanium, 6% aluminum (Al), and 4% vanadium (V). The latter is a variant of Ti gr 5 of higher purity and its improved mechanical properties are obtained by extra-low interstitial (ELI) carbon (C) and oxygen (O) and lower inclusions of iron.[11,12] More recently, a titanium-zirconium (Ti-Zr) alloy with 13% to 17% Zr has been introduced.[6,13]

To shorten the osseointegration period, various surface treatments have been developed producing different roughnesses and topography.[1,5,15-19] Two distinct

[a]Private practice, Barcelos, Portugal.
[b]Director of Research, MIS Implants Technologies, Bar Lev Industrial Park, Misgav, Israel.
[c]Professor, Department of Restorative Dentistry, University of Washington School of Dentistry, Seattle, Wash.

Clinical Implications

Commercially available implants made of distinct materials and with different surface treatments display diverse surface roughness, topographic features, and surface and subsurface compositions. High clinical success rates have been documented for these 3 implant systems, indicating that osseointegration can be obtained for a variety of surface states and materials.

methods, addition and subtraction, are in use. Treatment by addition includes plasma spraying of Ti or of hydroxyapatite, anodic oxidation,[3,4,12,20] and calcium phosphate deposition.[12] Treatment by subtraction includes airborne-particle abrasion with alumina, titania, or resorbable media and etching with various acidic mixtures, with or without prior airborne-particle abrasion.[17] Implant shape has evolved as well, from cylindrical to cylindroconical, and even conical starting from the implant neck.[21]

The design of the implant neck has also been a focus of change. First to be introduced were microthreads of various shapes and dimensions.[22] To create more room for bone at the crestal emergence of the implant neck, implants with neck shapes narrower than the implant body have been developed with the neck designed either as an inverse cone[23] or a triangle with 3 flat sides.[21,24]

The biological merits of the classical α-β Ti alloy compared with cp Ti have been researched, with either osseointegration or implant anchorage measured by using the reverse-torque method. Some authors reported advantages for cp Ti,[25-27] while others found no difference between cp Ti and Ti alloy.[28-33] These studies addressed machined or airborne-particle abraded surfaces of both materials, and, to the authors' knowledge, only one in vivo study has compared the airborne-particle abraded and etched (PAE) surfaces of both materials.[34] Some authors have claimed that PAE is typically not an appropriate treatment for the biphasic α-β Ti gr 5 alloy.[6]

Acid-etching of titanium leads to the production of small H^+ ions at the implant surface. Subsequently, the surface and the subsurface are enriched in H^+.[11,35,36] These ions diffuse toward the bulk and precipitate and form needles of Ti hydride (TiH_2).[11,36,37] Ions that remain at the implant surface create a layer of nonstoichiometric Ti hydride,[36,38] which interacts with the biological environment.[10,35,36] A high concentration of H^+ and needles of Ti hydride leads to so-called hydrogen embrittlement, which may reduce the mechanical properties of Ti and its alloys.[11]

The purpose of this in vitro study was to physically characterize and compare the surface and subsurface of 3 dental implant systems made of distinct materials with distinct surface treatments. The null hypothesis was that the surface roughness of these 3 clinically well-documented dental implant systems[39-41] would be similar.

MATERIAL AND METHODS

Three implants (n=3) from 3 commercially available dental implant systems were investigated. Information about the material and surface treatment was obtained from the respective company implant catalog and company websites: Group TG4AO included representative implants with a circular neck (3.5×8 mm) made of cp Ti gr 4 and treated by anodic oxidation (Nobel Replace Conical; Nobel Biocare).[4] Group TG23AE included implants with a triangular neck (3.9×8 mm) made of Ti gr 23, surface airborne-particle abraded with medical grade alumina, and etched in hot acids (V3; MIS). Group TG4AE included implants with a circular neck (3.3×8 mm) made of cold-worked cp Ti gr 4, surface airborne-particle abraded with large grit (0.25 to 0.50 mm) medical grade alumina, and etched in hot acids (BL; Institut Straumann AG).[6,17]

The surface roughness characteristics were determined by optical noncontact profilometry (Infinite Focus; Alicona Imaging) on a 250×250-μm field with a Gaussian filter of 50×50 μm.[15] The measurements were performed on 3 successive valleys between the threads of the 3 distinct implants. In accordance with the International Organization for Standardization (ISO 9693-1),[42] the following parameters were recorded: the mean arithmetic deviation roughness (S_a), the root mean square roughness (S_q), the average distance between the 5 highest peaks and 5 lowest valleys (S_{10z}), the skewness of the height distribution (S_{sk}), the kurtosis of the height distribution (S_{ku}), and the developed surface (S_{dr}).

The topographic features of the surface of the implants were examined with a scanning electron microscope (SEM) (Philips XL30; FEI Co) at 20 kV in the secondary electrons (SE) and back-scattered electrons (BSE) modes. Magnification ranged between ×20 and ×4000. Elements present on the surface and their concentration were identified by energy dispersive X-ray spectroscopy (EDS) with a silicon drift detector (XFlash 410-M; Bruker Nano) (<133 eV at MnKα).

The compounds present on the implants surfaces were determined by X-ray diffraction (XRD) by using a diffractometer (SmartLab 9KW; Rigaku) with a Cu Kα radiation (λ=1.5418 Å, U=40 kV, I=40 mA) and a secondary beam monochromator of graphite (002). The 2θ-scanned angle was 30 to 80 degrees, step size was

Table 1. Mean ±standard deviations roughness of 3 implant types

Type	S_a Arithmetic Mean Deviation of the Profile	S_q Root Mean Squared Height	S_{10z} Mean Height of 5 Highest Peaks and Valleys	S_{ks} Surface Skewness	S_{ku} Surface Kurtosis	S_{dr} Developed Interfacial Area Ratio
TG4AO	0.81 ±0.06	1.01 ±0.06	6.56 ±0.31	0.52 ±0.08	2.95 ±0.20	10.78 ±1.21
TG23AE	1.22 ±0.09	1.56 ±0.12	15.80 ±1.53	- 0.42 ±0.16	4.91 ±0.93	12.09 ±0.87
TG4AE	1.59 ±0.19	2.09 ±0.26	22.21 ±7.40	0.32 ±0.19	4.85 ±1.63	29.81 ±8.53
P	<.001	<.001	.001	.003	>.003	.001

Δ2θ=0.04 degrees, and counting time per step was 2 seconds. The implants were positioned perpendicular to the radiation beam. The results were compared with the information of pure powder standards (powder diffraction files) available from the International Center on Diffraction Data (ICDD).

The implants were embedded in resin, sectioned parallel to their long axis, and polished. The metallographic sections were examined under SEM/EDS and then etched with a lactic hydride reagent (5 mL lactic acid fresh and 5 mL of stock solution of 3 mL HF and 97 mL HNO_3)[43] to reveal the presence of TiH needles. The etched specimens were examined under the SEM at magnifications ranging from ×200 to ×13 000.

For group TG23AE, the possible enrichment from the etching process of an alloying element toward the surface and into the outer oxide layer was evaluated. A concentration profile of the alloying elements was obtained with a time-of-flight secondary ion mass spectrometry (ToF-SIMS) V mass spectrometer (IONTOF) equipped with a 25 KeV Bi^+ liquid metal ion gun (Bi^+ LMIG) as primary gun and a 1 KeV O_2^+ as the sputter ion beam in a positive polarity. Analysis and sputtered area were 80×80 μm and 300×300 μm. This method has a mass resolution of 0.00 × amu and submicrometer resolution imaging to map any mass number of interest. The roughness parameters of the 3 implant systems were compared by using the Kruskal-Wallis test for nonparametric data (α=.05).

RESULTS

The mean ±standard deviation roughness data are shown in Table 1. The S_a of groupTG4AO was 0.81 ±0.06 μm, below 1 μm; the S_a of the 2 other groups was within the 1- to 2-μm range. The S_q and S_{10z} were highest for group TG4AE. The S_{sk} was slightly negative for group TG23AE compared with the 2 other groups. The S_{ku} of group TG4AO was close to 3, and the surface was free of extreme peaks or valley features. With S_{ku} values approaching 5, the 2 PAE surfaces displayed a whole range of peaks and valleys. The developed surface (S_{dr}) was highest for group TG4AE. All surface parameters of the 3 implant groups were different, with means ±standard deviations presented in Table 1. The differences were statistically significant (*P*<.05).

The surface topography of each implant group appeared different. The surface of TG4AO obtained by anodic oxidation displayed a canyon-like structure of 3 to 12 μm of various heights with craters of 1 to 8 μm (Fig. 1A, 1D). The roughness was provided by the uneven structure. At higher magnification of ×8000, many cracks were seen running through the implant surface (Fig. 1D). The PAE surfaces of group TG23AE and TG4AE showed a macrotexture obtained by airborne-particle abrasion and a superimposed microtexture with pores carved by a strong acid attack. The macrotexture of group TG23AE was more rounded (Fig. 1B, 1E); for group TG4AE, it was more elongated and corresponded to the shape of the abrading material (Fig. 1C, 1F).

In terms of elemental composition, the presence of a high intensity peak of oxygen (O) and phosphorus (P) was detected in group TG4AO (Fig. 2A). The peak of O signals the presence of Ti oxide. The P peak corresponds to the incorporation of elements from the anodic oxidation bath that contained phosphoric acid.[4] The spectrum of group TG23AE showed a peak of Ti and Al alloying element. A peak specific to V did not appear because the Kα peak of V overlapped with the Kβ peak of Ti (Fig. 2B). For group TG4AE, the peak of Al was due to residue of the alumina abrading particles (Fig. 2C).

The XRD patterns of the 3 groups matched the peaks of the hexagonal α-Ti phase of powder diffraction file (PDF) #00-044-1294. However, each group displayed extra peaks corresponding to the presence of an additional compound on the surface. For group TG4AO, the extra peaks matched PDF #00-021-1272, corresponding to anatase, the tetragonal phase of Ti oxide (Fig. 3A). For group TG23AE, distribution of the α-Ti intensities differed from group TG4AO (Fig. 3B). The 3 additional peaks could not be identified with certainty. For group TG4AE, the extra peaks matched PDF #01-078-2216, which corresponded to cubic TiH_2 with its characteristic peaks at 41.0, 59.4, and 70.5 2θ degrees (Fig. 3C).

The metallographic sections of TG4AO displayed the anatase layer grown by anodic oxidation as greyish, less dense than the Ti substrate (Fig. 4). The thickness of the oxide varied from approximately 3 to 13 μm, with pores

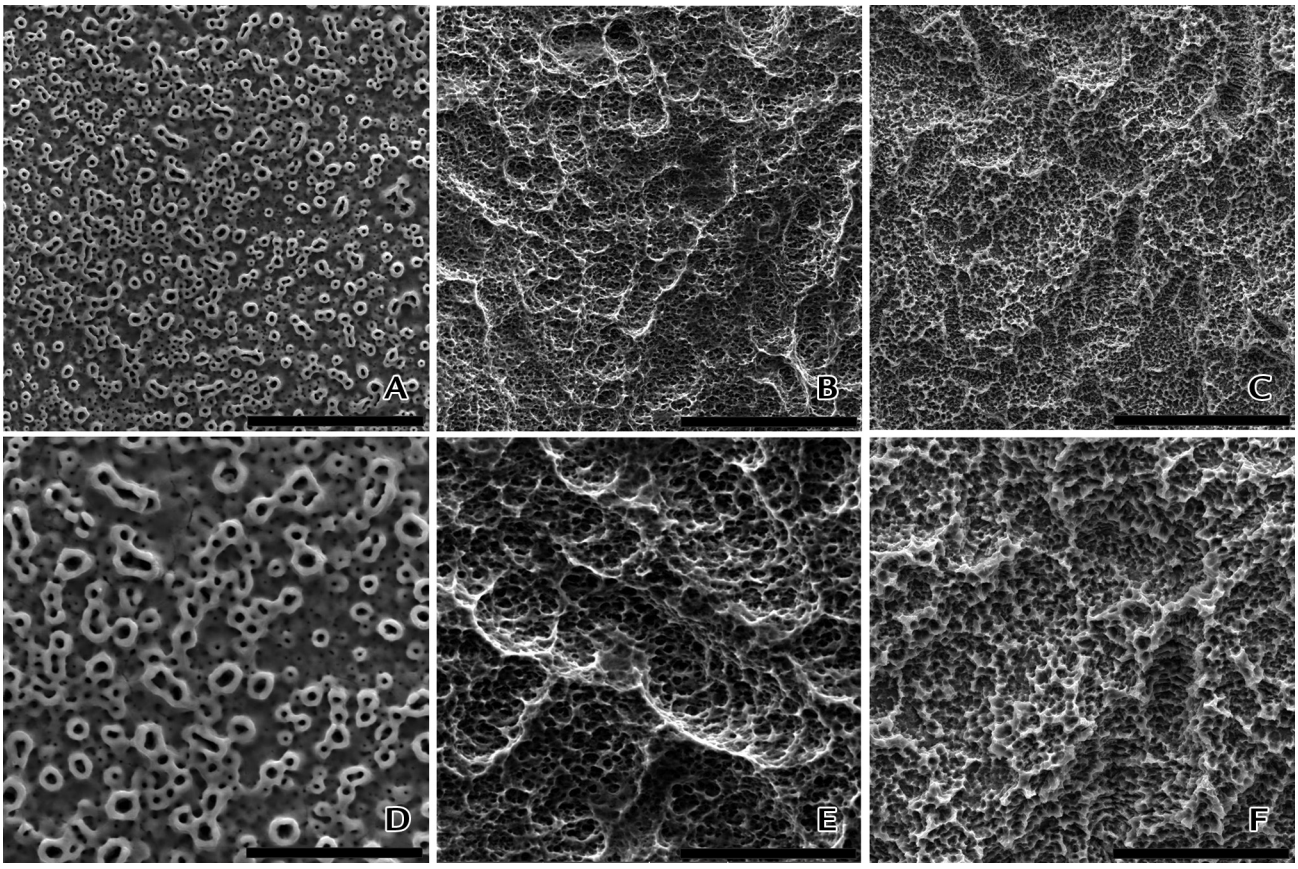

Figure 1. Surface characteristics of implant of each of groups tested. A, Surface of TG4AO (NobelReplace Conical; Nobel Biocare) showing canyon-like structure providing roughness effect (original magnification ×1000, bar=100 μm). B, Surface of TG23AE (V3; MIS) showing rounded macrostructures superimposed by microtexture with pores (original magnification ×1000, bar=100 μm). C, Surface of TG4AE (BL; Straumann AB) showing elongated macrostructures with microtexture with pores (original magnification ×1000, bar=100 μm). D, Closer view of TG4AO. Note random distribution of canyon-like structure with craters and cracks running over oxide layer (original magnification ×2000, bar=50 μm). E, Closer view of TG23AE. Micropores carved by acid on top of macrostructure produced by airborne-particle abrasion (original magnification ×2000, bar=50 μm). F, Closer view of TG4AE. Superimposed micropores on top of macrotextured surface appear numerous and sharp.

and cracks running within the bulk of the oxide (Fig. 4). For group TG23AE, white grains were distributed among a dark Ti matrix (Fig. 5A). Elemental analysis of the white grains and the matrix showed different concentrations of the alloyed elements (Fig. 5B). The mean Al and V weight% composition of the white grains was 4.6% and 7.4%, and, for the Ti matrix, it was 5.3% and 3.2%. The white grains were richer in V and deprived of Al and belonged to the β-phase of the alloy. The dark matrix corresponded to the α-phase, which was richer in Al and deprived of V.

Etching revealed TiH needles on group TG4AE only (Fig. 6A). The thin needles were approximately 1.5 to 40 μm long. At the thread level, TiH needles were longer and more numerous and propagated deeper inside the implant bulk for up to approximately 360 μm. In the valleys between the threads, their diffusion depth was limited to approximately 100 μm (Fig. 6). Some TiH needles were directly perpendicular to the implant surface (Fig. 6C).

Depth profiling was performed for group TG23AE exclusively to evaluate the V enrichment of the surface as suggested by Salaucic et al.[6] From the bulk toward the surface of the oxide layer, the concentration of Al and V decreased (Fig. 7). The Ti oxide layer was depleted in these elements. No enrichment of any alloying element was observed.

DISCUSSION

The present study aimed to characterize the surface of 3 commercially available dental implants systems that differ by material, surface treatment, and surface composition. The null hypothesis that these implant surfaces would have similar implant roughness characteristics was rejected.

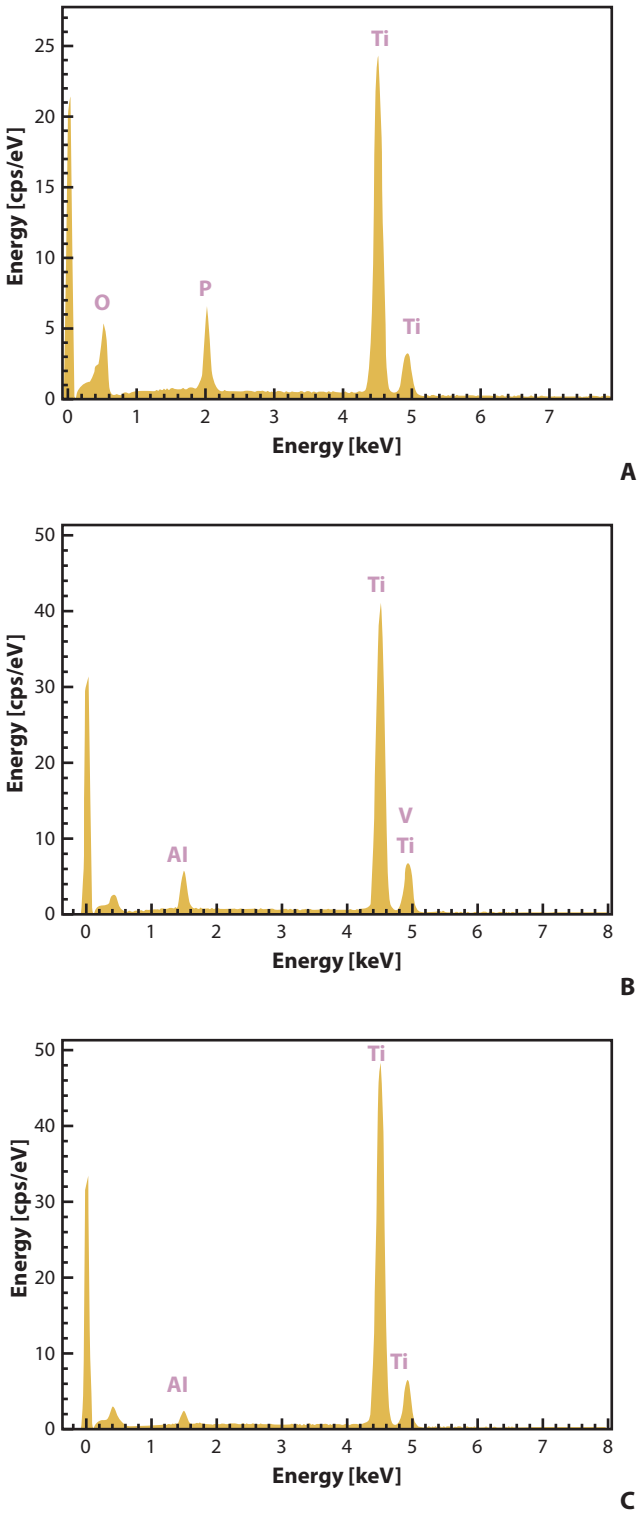

Figure 2. Elemental analysis of surface. A, Spectrum of TG4AO. In addition to peaks of Ti, note presence of peak of O that indicates presence of oxide layer; P peak comes from anodization bath that contained phosphoric acid. B, Spectrum of TG23AE. In addition to peaks of Ti, note presence of significant peak of Al. Peak specific to V not visible because it overlaps β-peak of Ti. C, Spectrum of TG4AE. In addition to peaks of Ti, note presence of small peak of Al coming from alumina particles that remained on implant surface.

Group TG4AO had the topographic feature of a canyon-like structure with open craters. Its roughness was the lowest among the investigated groups. With a S_a of 0.81 μm, it can be categorized as having a minimally rough surface.[5,16] Other roughness values for this surface were documented and are either consistent with the present findings, 0.87 μm or rougher (1.17 μm and 1.35 μm) depending on the measuring devices.[4,8,9] The grown oxide layer is made of well-crystalized anatase of variable thickness from 3 to 15 μm (Fig. 4). The signal of the α-Ti phase was unexpectedly strong, while the oxide one was rather weak. This was caused by the highly variable thickness of the oxide that allowed the underlying substrate to strongly contribute to the diffraction signal. An oxide thickness of 5.7 to 9.3 μm has previously been reported.[4] The present study characterized it both as thinner and thicker. The oxide layer was porous with many cracks, probably because of high internal residual stress. This may explain why flakes of the oxide layer have been observed.[44] The depth of the open 1- to 8-μm craters were reaching 6 to 7 μm, which allows bone ingrowth.[20] Despite a S_a <1 μm, similar to the roughness measured on machined implants,[16] this topographic feature may also explain why surface cleaning in the presence of plaque or infection is more difficult than for other airborne-particle abraded or PAE surfaces.[45]

The surface of groups TG23AE and TG4AE looked like typical PAE-treated titanium implants with a macrotexture and microtexture.[6,17,36,44] The macrotexture of group TG23AE was rather round in shape (Figs. 2B, 4E), while it was elongated for group TG4AE (Figs. 2C, 4F). This difference might have been a result of the shape and granulometry of the abrasion material. However, it may also be because of the distinct acid mixtures involved.

The spatial roughness parameters of group TG4AE were higher than for group TG23AE, and the S_{dr} was approximately 2.5 times higher (Table 1), probably because of deeper pores carved by the acid mixture. It should be interesting to verify if surfaces with deeper pores, and a larger S_{dr} may be more challenging to maintain in situations of peri-implantitis.

A marked difference between the PAE groups was that the etching modified the surface composition of group TG23AE but not of group TG4AE, which was consistent with previous findings.[36] Acid etching leads to the diffusion of small H^+ ions into the material undergoing the strong corrosion process. On cp Ti, the

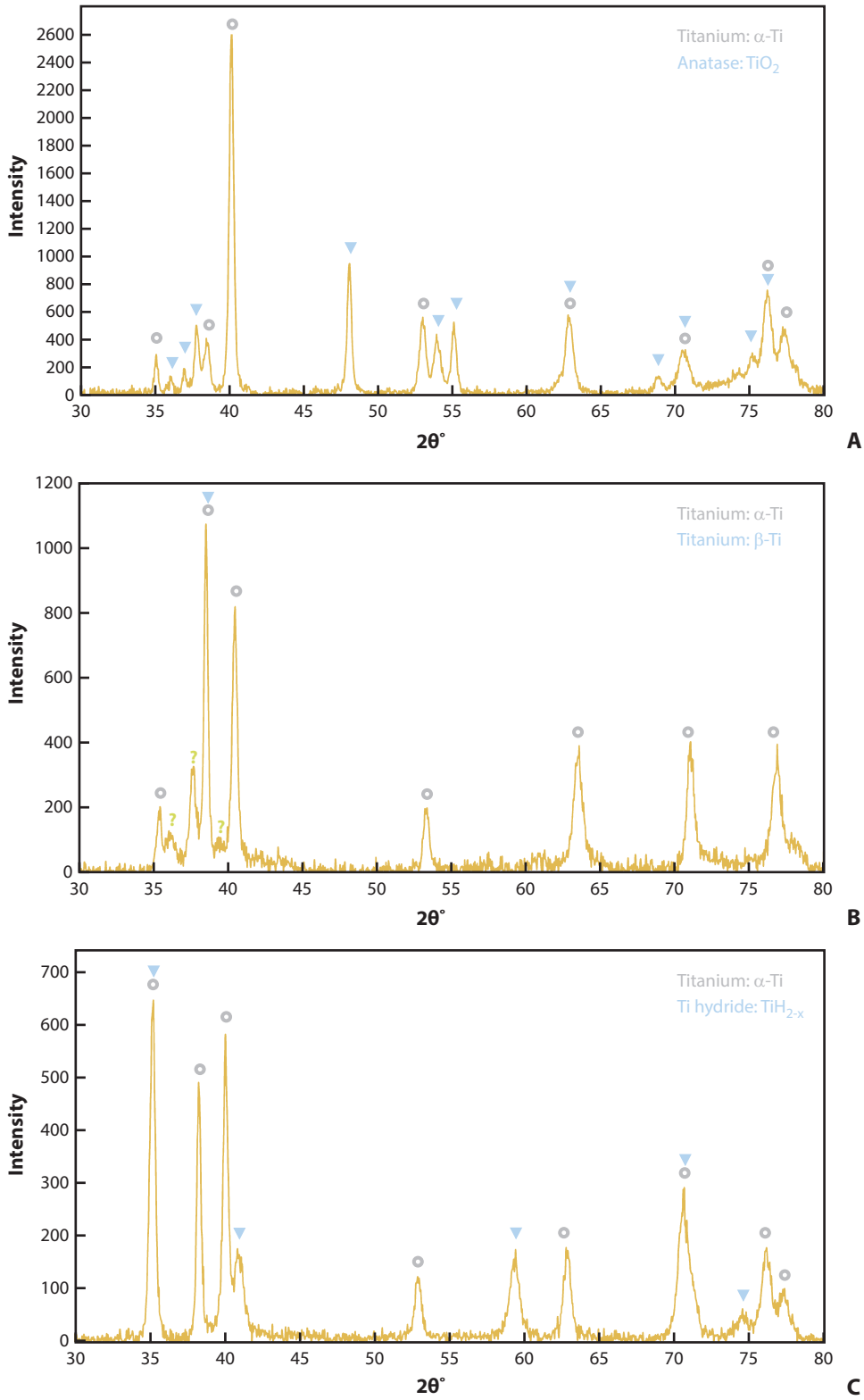

Figure 3. X-ray diffraction patterns of implant surfaces. A, Spectrum of TG4AO. Numerous additional peaks that do not belong to α-Ti fitting anatase, rhomboid Ti oxide. B, Spectrum of TG23AE. Peaks belonging to α-Ti where found and additional ones not identified. Main peak of cubic β-Ti phase overlapping with α-Ti peak (002) at 38.44 degrees. C, Spectrum of TG4AE. Peaks not belonging to α-Ti fitting with cubic TiH_2.

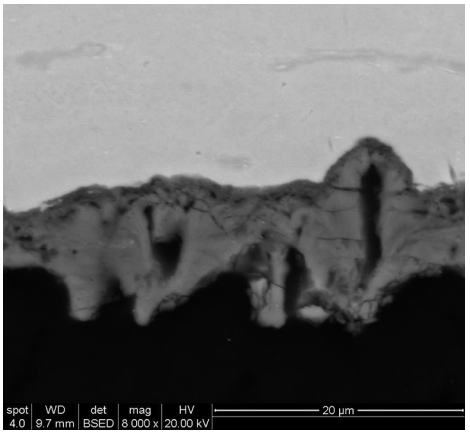

Figure 4. Backscattered scanning electron micrographs of metallographic sections of TG4AO. Original magnification ×8000. Oxide layer darker than Ti bulk material, indicating that atomic weight (or Z-contrast information) of oxide is below that of Ti bulk material. Darker image indicates lighter material providing signal. Thickness of oxide layer uneven, from approximately 3 to 12 µm. Canyon-like structure delimits craters for possible bone ingrowth. Oxide porous and cracks running in grown anatase.

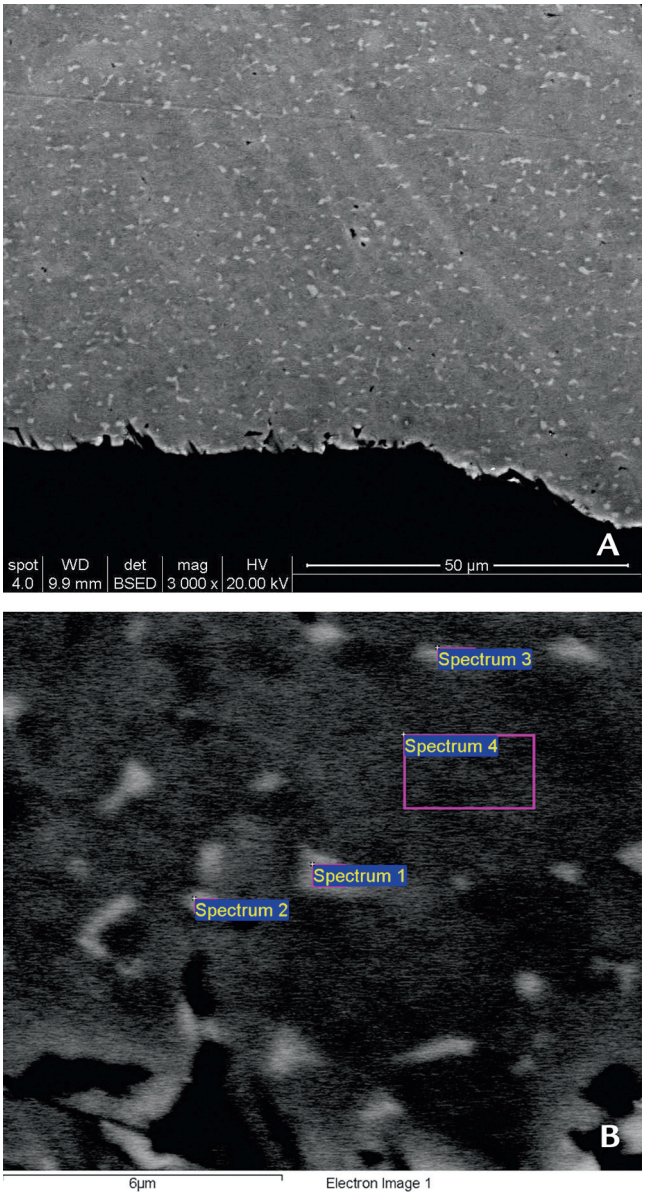

Figure 5. Backscattered scanning electron micrographs of metallographic sections of TG23AE. A, Original magnification ×3000. Note presence of white spots of β-Ti phase denser than matrix. B, Original magnification ×1000. Location of white β-Ti grains and α-Ti matrix where elemental composition analyzed by energy dispersive X-ray spectroscopy.

diffusing H^+ ions forms a TiH layer beneath the implant surface. When the etching conditions are strong, TiH concentration on the surface as determined by XRD can reach 19% to 37%. However, when weaker, it is in the 5% to 8% range.[36] H solubility is limited in the hexagonal close packed (hcp) structure of the α-Ti phase used for group TG4AE; above 20 ppm, H precipitates into TiH,[37] and the α-Ti phase coexists with a nonstoichiometric deficient dihydride, the δ-TiH_{2-x} phase.[38] In contrast, no TiH compound could be assessed on the surface of the α-β Ti alloy because H solubility in the alloy is much higher. The body-centered cubic structure (bcc) of the β-Ti phase accommodates many more interstitial elements than the hcp α-Ti phase. Shih and Birnbaum[46] reported that loading the biphasic alloy with 50 atomic% H did not lead to TiH precipitation. The presence of TiH on the surface has been reported to positively affect the bone response,[10] but others found no benefit.[35]

For group TG4AE, the increase of H concentration at the implant surface led to the precipitation of thin TiH needles (Fig. 6) that were not evenly distributed. The needles were more numerous at the thread level than at the valleys between the threads and propagated deeper in the material, up to approximately 360 µm at the thread level compared with approximately 100 µm in the valleys between the threads. The needles close to the surface were smaller than the deeper ones (Fig. 6B), and, in the valleys, some needles were directly perpendicular to the surface and may serve a notch starting point for fissure propagation. Cold-worked cp Ti is especially sensitive to H embrittlement, and the combination of notches and H embrittlement might cause long-term mechanical concern.[11]

Time-of-flight secondary ion mass spectrometry (ToF-SIMS) depth profiling was performed on group TG23AE to address the issue of the appropriateness of PAE for Ti alloyed implants.[6] Enrichment of any of the alloying elements at the implant surface was not

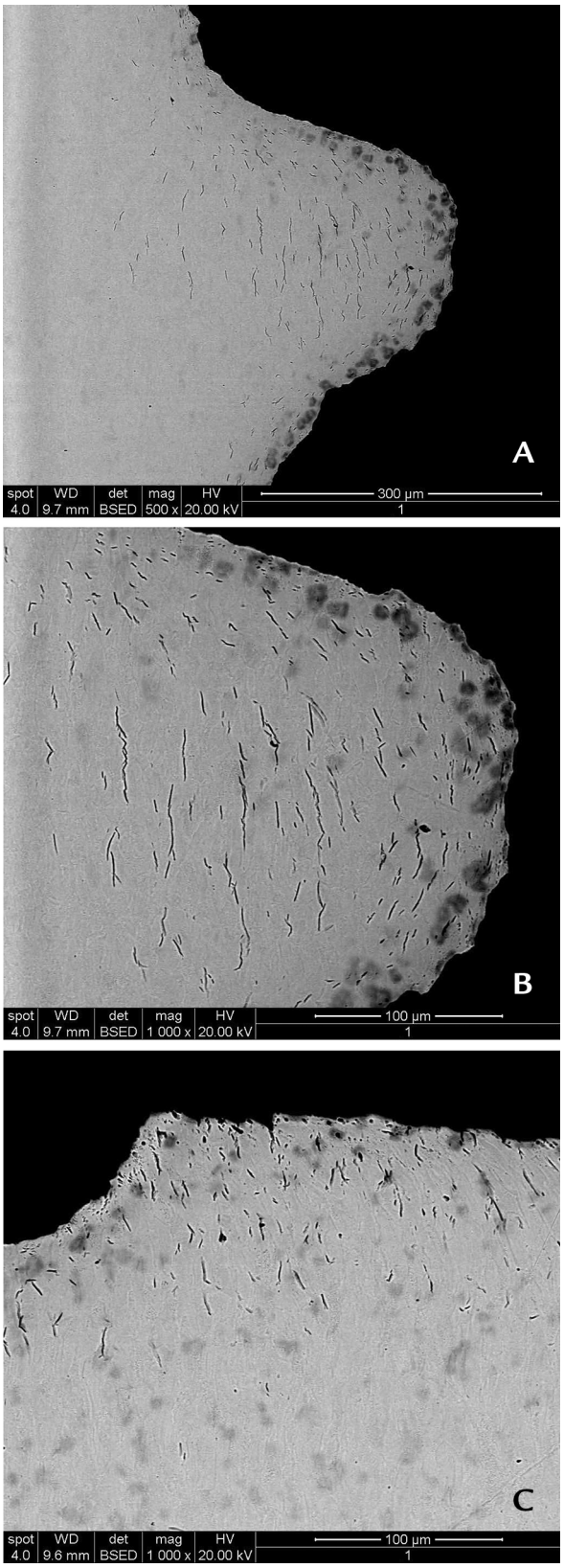

Figure 6. Backscattered scanning electron micrographs of metallographic sections of TG4AE after etching. A, Original magnification ×500. Thread showing presence of TiH needles. At thread level, needles more numerous than between threads and their penetration depth up to 360 µm. B, Original magnification ×1000. Various sizes of TiH needles, shorter when closer to implant surface. C, Original magnification ×1000 in valley between threads. Penetration depth of TiH needles up to 100 µm. Note presence of some needles perpendicular to implant surface.

observed (Fig. 7). Moreover, depletion of Al and V occurred while approaching the surface from the bulk side. Szmukler-Moncler et al[7] investigated the etched surface of a Ti gr 5 implant and described a similar pattern of macrotexture and microtexture. Depth profiling was performed by AES and Ar^+ sputtering. However, no enrichment of either Al or V was found at the surface or the subsurface. Noteworthy, the etching conditions are strong enough to simultaneously dissolve the α and the β phases. When the etching conditions are weaker, the acid carves pores into the alloy and removes preferentially the α-Ti matrix. The β-Ti phase that is more corrosion resistant remains on the etched surface.[36] This phase is richer in V and denser than the matrix. The β-Ti grains observed in the backscattered mode under the SEM at ×3000 magnification appeared white and sharp, looking similar to remaining airborne-abraded alumina particles.[14,36,44]

Pimenta et al[34] compared the osseointegration of these 3 implant groups in a rabbit tibia model 6 weeks after implant placement. Despite the differences of surface topography and surface composition, the level of osseointegration was similar for all groups. Bone-implant contact of the group TG4AO was 58.1 ±1.6%, for group TG23AE 59 ±2.0%, and for group TG4AE 58.7 ±1.8%, which was not statistically significantly different. Therefore, in contrast with Salaucic et al,[6] it may be concluded that PAE is an appropriate treatment for implants made of α-β Ti alloy when an adequate etching procedure is implemented.

Limitations of this study included the relatively limited sample size. Further research of more implant systems with a larger sample size should be performed with uniform physical methods.

CONCLUSIONS

Based on the findings of this in vitro study the following conclusions were drawn:

1. The 3 implant groups presented distinct characteristics in terms of materials, surface topography, and surface composition.
2. Airborne-particle abrasion and etching of the biphasic Ti gr 23 was an appropriate texturing process. The α-Ti and the β-Ti phases were concomitantly dissolved, and the surface presented the typical macroroughness and microroughness

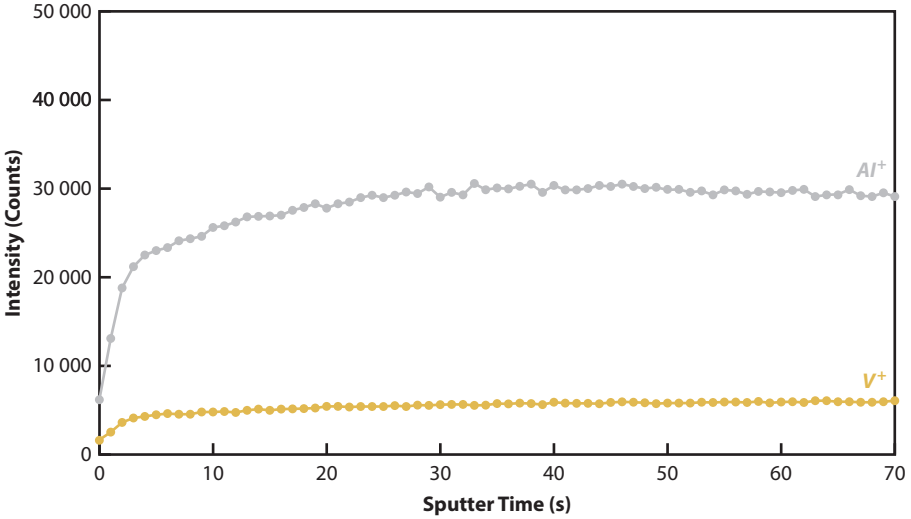

Figure 7. Time-of-flight secondary ion mass spectrometry depth profiling of Al and V. Note concentration reduction of Al^+ and V^+ from bulk toward surface. No Al or V signal augmentation close to surface or within oxide layer.

observed on PAE cp Ti implant surfaces without β-Ti phase residues.

REFERENCES

1. Buser D, Nydegger T, Hirt HP, Cochran DL, Nolte LP. Removal torque values of titanium implants in the maxilla of miniature pigs. Int J Oral Maxillofac Implants 1998;13:611-9.
2. Tait RT, Berckmans BN, Ross TW, Mayfield RL. Surface treatment process for implants made of titanium alloy 2004. US patent 0265,780.
3. Sul YT, Johansson C, Albrektsson T. Which surface properties enhance bone response to implants? Comparison of oxidized magnesium, TiUnite, and osseotite implant surfaces. Int J Prosthodont 2006;19:319-28.
4. Sul YT, Byon E, Wennerberg A. Surface characteristics of electrochemically oxidized implants and acid-etched implants: surface chemistry, morphology, pore configurations, oxide thickness, crystal structure, and roughness. Int J Oral Maxillofac Implants 2008;23:631-40.
5. Wennerberg A, Albrektsson T. Effects of titanium surface topography on bone integration: a systematic review. Clin Oral Implants Res 2009;20: 172-84.
6. Saulacic N, Bosshardt DD, Bornstein MM, Berner S, Buser D. Bone apposition to a titanium-zirconium alloy implant, as compared to two other titanium-containing implants. Eur Cell Mater 2012;23:273-86.
7. Szmukler-Moncler S, Blus C, Morales Schwarz D, Orrù G. Characterization of a macro- and micro-textured titanium grade 5 alloy surface obtained by etching only without sandblasting. Materials (Basel) 2020;13:5074.
8. Ivanoff CJ, Widmark G, Johansson C, Wennerberg A. Histologic evaluation of bone response to oxidized and turned titanium micro-implants in human jawbone. Int J Oral Maxillofac Implants 2003;18:341-8.
9. Shibli JA, Grassi S, de Figueiredo LC, Feres M, Marcantonio E Jr, Iezzi G, et al. Influence of implant surface topography on early osseointegration: a histological study in human jaws. J Biomed Mater Res B Appl Biomater 2007;80:377-85.
10. Cheng Z, Zhang F, He F, Zhang L, Guo C, Zhao S, et al. Osseointegration of titanium implants with a roughened surface containing hydride ion in a rabbit model. Oral Surg Oral Med Oral Pathol Oral Radiol Endod 2010;110: e5-12.
11. Donachie MJ Jr. Titanium: a technical guide. 2nd ed. Materials Park, OH: ASM International; 2000. p. 85-94.
12. Brunette DM, Tengvall P, Textor M, Thomsen P. Titanium in medicine. Material science, surface science, engineering, biological responses and medical applications. Berlin: Springer; 2001. p. 25-52.
13. Bernhard N, Berner S, De Wild M, Wieland M. The binary TiZr alloy. A newly developed Ti alloy for use in dental implants. Forum Implantologicum 2009;5: 30-9.
14. Sittig C, Textor M, Spencer ND, Wieland M, Vallotton PH. Surface characterization of implant materials cp Ti, Ti-6Al-7Nb and Ti-6Al-4V with different pretreatments. J Mater Sci Mater Med 1999;10:35-46.
15. Wennerberg A, Albrektsson T. Suggested guidelines for the topographic evaluation of implant surfaces. Int J Oral Maxillofac Implants 2000;15:331-44.
16. Albrektsson T, Wennerberg A. Oral implant surfaces: part 1 - review focusing on topographic and chemical properties of different surfaces and in vivo responses to them. Int J Prosthodont 2004;17:536-43.
17. Szmukler-Moncler S, Testori T, Bernard JP. Etched implants: a comparative surface analysis of four implant systems. J Biomed Mater Res B Appl Biomater 2004;69:46-57.
18. Weibrich G, Kleis W, Buch RSR, Hansen T, Streckbein P. Bone remodeling around dental implants surfaces. J Dent Implantol (ZZI) 2009;3:238-49.
19. Gehrke SA, Marin GW. Biomechanical evaluation of dental implants with three different designs: removal torque and resonance frequency analysis in rabbits. Ann Anat 2015;199:30-5.
20. Schüpbach P, Glauser R, Rocci A, Martignoni M, Sennerby L, Lundgren A, et al. The human bone-oxidized titanium implant interface: a light microscopic, scanning electron microscopic, back-scatter scanning electron microscopic, and energy-dispersive x-ray study of clinically retrieved dental implants. Clin Implant Dent Relat Res 2005;7 Suppl 1:S36-43.
21. Davarpanah D, Szmukler-Moncler S, Rajzbaum P, Davarpanah K, Bichacho N, Van Dooren E. ImplantoLOGIC. Treatment planning and decision making. Paris: Espace ID; 2018. p. 18-22.
22. Messias A, Nicolau P, Guerra F. Titanium dental implants with different collar design and surface modifications: a systematic review on survival rates and marginal bone levels. Clin Oral Implants Res 2019;30:20-48.
23. Irinakis T, Wiebe C. Clinical evaluation of the NobelActive implant system: a case series of 107 consecutively placed implants and a review of the implant features. J Oral Implantol 2009;35:283-8.
24. Sanz-Martin I, Vignoletti F, Nuñez J, Permuy M, Muñoz F, Sanz-Esporrín J, et al. Hard and soft tissue integration of immediate and delayed implants with a modified coronal macro-design: histological, micro-CT and volumetric soft tissue changes from a pre-clinical in vivo study. J Clin Periodontol 2017;44:842-53.
25. Johansson CB, Han CH, Wennerberg A, Albrektsson T. A quantitative comparison of machined commercially pure titanium and titanium-aluminum-vanadium implants in rabbit bone. Int J Oral Maxillofac Implants 1998;13:315-21.
26. Han CH, Johansson CB, Wennerberg A, Albrektsson T. Quantitative and qualitative investigations of surface enlarged titanium and titanium alloy implants. Clin Oral Implants Res 1998;9:1-10.
27. Stenport VF, Johansson CB. Evaluation of bone tissue integration to pure and alloyed titanium implants. Clin Implant Dent Relat Res 2008;10:191-9.
28. Carr AB, Gerard DA, Larsen PE. Quantitative histomorphometric description of implant anchorage for three types of dental implants following 3 months of healing in baboons. Int J Oral Maxillofac Implants 1997;12:777-84.
29. Carr AB, Gerard DA, Larsen PE. Histomorphometric analysis of implant anchorage for 3 types of dental implants following 6 months of healing in baboon jaws. Int J Oral Maxillofac Implants 2000;15: 785-91.
30. Carr AB, Larsen PE, Gerard DA. Histomorphometric comparison of implant anchorage for two types of dental implants after 3 and 6 months' healing in baboon jaws. J Prosthet Dent 2001;85:276-80.

31. De Maeztu MA, Braceras I, Álava JI, Recio C, Piñera M, Gay-Escoda C. Human study of ion implantation as a surface treatment for dental implants. Int J Oral Maxillofac Surg 2013;42:891-6.
32. Shah FA, Trobos M, Thomsen P, Palmquist A. Commercially pure titanium (cp-Ti) versus titanium alloy (Ti6Al4V) materials as bone anchored implants - is one truly better than the other? Mater Sci Eng C Mater Biol Appl 2016;62:960-6.
33. Cordeiro JM, Barão VAR. Is there scientific evidence favoring the substitution of commercially pure titanium with titanium alloys for the manufacture of dental implants? Mater Sci Eng C Mater Biol Appl 2017;71:1201-15.
34. Pimenta J, Aramburú JS Jr, Dedavid BA, Gehrke SA. In vivo comparative analysis of the osseointegration potential among three leading implant brands in the European market. INPerio 2018;3:274-82.
35. Perrin D, Szmukler-Moncler S, Echikou C, Pointaire P, Bernard JP. Bone response to alteration of surface topography and surface composition of sandblasted and acid etched (SLA) implants. Clin Oral Implants Res 2002;13:465-9.
36. Szmukler-Moncler S, Bischof M, Nedir R, Ermrich M. Titanium hydride and hydrogen concentration in acid-etched commercially pure titanium and titanium alloy implants: a comparative analysis of five implant systems. Clin Oral Implants Res 2010;21:944-50.
37. Livanov VA, Bukhanova AA, Kolachev BA. Hydrogen in titanium. New York: D Davey & Co; 1962. p. 35-60.
38. Dantzer P. High temperature thermodynamics of H2 and D2 in titanium and in dilute titanium oxygen solid solutions. J Phys Chem Solids 1983;44:913-23.
39. Horwitz J, Machtei EE. Immediate and delayed restoration of dental implants in patients with a history of periodontitis: a prospective evaluation up to 5 years. Int J Oral Maxillofac Implants 2012;27:1137-43.
40. Mozzati M, Gallesio G, Del Fabbro M. Long-term (9-12 years) outcomes of titanium implants with an oxidized surface: a retrospective investigation on 209 implants. J Oral Implantol 2015;41:437-43.
41. Kim S, Jung UW, Cho KS, Lee JS. Retrospective radiographic observational study of 1692 Straumann tissue-level dental implants over 10 years: I. Implant survival and loss pattern. Clin Implant Dent Relat Res 2018;20:860-6.
42. International Organization for Standardization. ISO 9693-1. Dentistry compatibility testing. Part 1: metal-ceramic systems. Geneva: International Organization for Standardization; 2012. ISO Store Order: OP-184149 (Date: 2017-06-09). Available at: http://www.iso.org/iso/home.html.
43. Gammon LM, Briggs RD, Packard JM, Batson KW, Boyer R, Domby CW. Metallography and microstructures of titanium and its alloys. ASM handbook. Materials Park, OH: ASM International; 2004. p. 899-917.
44. Davarpanah M, Szmukler-Moncler S, Rajzbaum P. Manuel d'implantologie clinique. Consolidation des savoirs et ouvertures sur l'avenir. 4th ed. Paris: Editions CdP; 2018. p. 72-84.
45. Albouy JP, Abrahamsson I, Persson LG, Berglundh T. Implant surface characteristics influence the outcome of treatment of peri-implantitis: an experimental study in dogs. J Clin Periodontol 2011;38:58-64.
46. Shih DS, Birnbaum HK. Evidence of fcc titanium hydride formation in titanium alloy: an X-ray diffraction study. Scripta Metallurgica 1986;20:1261-4.

Corresponding author:
Dr João Pimenta
Rua Simplício de Sousa 24, Barcelos P-4754
PORTUGAL
Email: pimenta57@hotmail.com

Acknowledgments
The authors thank Boris Gishvoliner for the SEM macrographs, Dr Keren Zohar-Hauber for the preparation of the metallographic sections, and Dr Rotem Strassberg for the TOF-SIMS analysis.

CRediT authorship contribution statement
João Pimenta: Conceptualization, Resources, Writing - review & editing. **Serge Szmukler-Moncler:** Conceptualization, Resources, Data curation, Writing - review & editing. **Ariel Raigrodski:** Writing - review & editing, Visualization.

https://doi.org/10.1016/j.prosdent.2020.11.015